

Fault Diagnosis Method for Open-circuit Faults in NPC Three-level Inverter based on WKCNN

Guozheng Zhang, *Member, CES and IEEE*, Menghui Li, Xin Gu, *Member, IEEE*, and Wei Chen, *Member, IEEE*

Abstract—With the increasing demand for high reliability and availability in power conversion equipment within power electronics systems, the fault diagnosis of neutral-point-clamped (NPC) three-level inverters has garnered widespread attention. To address the challenges of fault feature extraction, this article proposes an end-to-end diagnostic approach based on a wavelet kernel convolutional neural network (WKCNN), capable of extracting multi-scale features from current signals to significantly enhance diagnostic accuracy. This method directly uses raw three-phase current signals as input, applying wavelet kernel convolution to automatically capture frequency-domain fault features, combined with a Softmax classifier optimized by the Adam algorithm to achieve fault diagnosis for NPC three-level inverters. Experimental results under various operating conditions demonstrate that this approach maintains robust diagnostic accuracy across multiple fault scenarios, with comparative analysis further confirming its advantages in diagnostic efficiency and performance over traditional machine learning and other deep learning methods.

Index Terms—NPC three-level inverter, Open-circuit fault, Wavelet transform, Convolutional neural network, End-to-end.

I. INTRODUCTION

THE neutral-point-clamped (NPC) three-level inverter is widely used in medium and high-voltage applications, such as renewable energy generation [1], industrial drives, and power transmission systems. It offers advantages such as low output harmonic distortion and reduced switching losses [2]. However, due to the complex topology and multi-device parallel design of NPC inverters, they are prone to failure of switching components during actual operation. Fault diagnosis technology is essential to detect and locate these faults in real-time, thereby preventing equipment damage and enhancing the reliability and safety of the system. Consequently, research on fault diagnosis for NPC three-level inverters holds significant engineering application value and economic benefits.

Manuscript received January 14, 2025; revised March 15, 2025; accepted March 27, 2025. Date of publication June 25, 2025; Date of current version April 14, 2025.

This work was supported in part by Zhejiang Provincial “Pioneer” and “Leading Goose” R&D Program of China under Grant 2024C01014 and in part by the National Natural Science Foundation of China under Grant 52177055. (*Corresponding author: Xin Gu*).

G. Z. Zhang, M. H. Li, X. Gu, and W. Chen are with the School of Electrical Engineering, Tiangong University, Tianjin 300387, China (e-mail: zhanggz@tju.edu.cn; limenghui@tiangong.edu.cn; guxin@tiangong.edu.cn; chen_wei@tiangong.edu.cn).

Digital Object Identifier 10.30941/CESTEMS.2025.00012

Fault diagnosis methods for open-circuit faults in inverters are generally categorized into model-based methods, signal analysis-based methods, and artificial intelligence-based methods [3]. Model-based methods construct a mathematical model of the inverter and use observers to estimate key parameters such as three-phase currents. Faults are diagnosed by comparing observer residuals with predefined thresholds. A method that combines model predictive control (MPC) with a mixed logical dynamic (MLD) model is proposed in [4], where phase currents are predicted, and logical vectors are employed to locate faulty switches. [5] uses a Luenberger observer to estimate the actual circulating current in parallel inverters, compare it with the predicted current, and generate a residual signal for detecting and locating faulty switches. [6] utilizes current residuals obtained through a Luenberger observer as diagnostic variables, which are then comprehensively evaluated by a machine learning model to classify fault modes based on the residual distributions. [7] proposes a fault diagnosis method for three-level converters based on voltage difference residuals. A rapid diagnostic method based on the switching function model is presented in [8], which detects open-circuit faults by analyzing changes in the inverter’s switching state, and achieves fault detection without the need for extra sensors. Model-based methods are generally robust to variations in load and speed, but they rely heavily on the precision of the system model. The mathematical models used for motor drives are also more complex.

Signal-based methods identify faults by analyzing changes in current or voltage signals from the inverter output. In [9], Concordia transformation is used to convert three-phase currents into two-phase currents. Faults are detected by analyzing changes in the shape and angle of the current trajectory. In [10], an analysis method based on symmetric and DC components is used. By calculating the ratio of positive and negative sequence components of phase currents and the polarity of the DC component, single or multiple open-circuit faults in a permanent magnet synchronous motor (PMSM) drive system are detected. In [11], a method is proposed to diagnose single and double open-circuit faults in voltage source inverters by analyzing line voltage magnitude variations. [12] proposes a method to identify and differentiate open-circuit faults in upper switches, lower switches, and clamping diodes. It achieves this by analyzing the distortion characteristics of output currents based on the polarity changes during positive and negative half cycles. In

[13], open-circuit faults in inverters are detected by analyzing the current vector trajectory and instantaneous frequency. Signal-based diagnostic methods may face challenges when system parameters change. Original thresholds might become invalid, often requiring re-tuning to maintain diagnostic accuracy. This reliance on thresholds increases complexity and reduces its robustness under varying conditions.

In recent years, with the rapid development of machine learning technologies, artificial intelligence-based fault diagnosis methods have increasingly become a popular research direction. The AI-based methods primarily achieve intelligent decision-making by hierarchically processing fault data, extracting key features, and mapping these features to fault categories [14]. In [15], a fault diagnosis method based on energy spectral entropy and wavelet neural networks is presented, where wavelet packet decomposition is used to extract voltage signal features, and an adaptive wavelet neural network is employed for fault classification. An approach is proposed in [16], which utilizes a hybrid convolutional neural network (CNN) to extract features through both one-dimensional (1D CNN) and two-dimensional convolutional networks (2D CNN), subsequently fusing these features to diagnose faults in three-phase inverters. In [17], signals are pre-processed via Fourier transform, and feature extraction and dimensionality reduction are carried out using relative principle component analysis (RPCA), followed by fault classification using a support vector machine (SVM). [18] proposes a CNN-based method for fault detection. In [19], a diagnostic approach for detecting both single and double open-circuit faults under rectification and active inverter states is introduced. An improved 1D CNN-based method is suggested in [20], where features are extracted from the output current signals of NPC-type inverters, and adaptive optimization algorithms are used to locate faulty switches. In [21], a wavelet CNN is employed for open-circuit fault diagnosis by extracting features from the normalized current vector trajectory plots, effectively diagnosing open-circuit faults in PMSM drive systems. [22] proposes a method for diagnosing early inter-turn short-circuit faults in motors. The method uses feature-layer multi-source signal fusion and an improved CNN. [23] proposes a fault diagnosis method for three-phase motors. The method is based on game mapping learning and multi-sensor information fusion. Complementary information from multiple sensors is fused at the feature or decision level to improve diagnostic accuracy. [24] proposes a method for bearing fault diagnosis. The method uses a dual-channel transformer and Swin transformer V2. A one-dimensional transformer directly processes the raw vibration signal. An improved Swin transformer V2 model extracts image spatial features. The architecture fuses time-domain and frequency-domain information to enhance fault features. [25] proposes an end-to-end improved CNN for fault diagnosis of three-phase voltage-source inverters. A wide first-layer convolution kernel is used to enhance feature extraction. Global max pooling replaces the fully connected layer to reduce the parameter count and computational cost. However, the fixed large convolution kernel lacks flexibility

in extracting features at different scales.

Traditional neural network models often rely on manual feature extraction, which is labor-intensive, time-consuming, and may introduce subjectivity and inaccuracy in feature selection. Furthermore, under complex and varying operating conditions, manually extracted features may not sufficiently reflect the fault characteristics of the system, thus affecting the accuracy and effectiveness of the diagnosis. Although powerful automatic feature extraction capability is possessed by deep learning models, complex preprocessing is still employed by many deep networks in fault diagnosis tasks. Computational complexity is thereby increased. In addition, network architectures are sometimes designed to be overly complex, and an excessive number of parameters is employed. Consequently, computational cost is elevated and applicability is limited to specific operating conditions.

To address the issues mentioned above, this article proposes a novel NPC three-level inverter open-circuit fault diagnosis model with end-to-end diagnostic capability. The model utilizes a wavelet kernel convolutional network (WKCNN), which directly processes output current data under varying operating conditions to classify faults. In contrast to conventional wavelet neural networks, deep fusion is achieved in WKCNN between parameterized dynamic wavelet kernels and a deep convolutional architecture. Learnable scale factors and translation factors are introduced to dynamically generate wavelet kernels, thereby replacing the conventional fixed wavelet basis. The wavelet time-frequency resolution is adaptively adjusted by backpropagation. An end-to-end optimization mechanism is combined, which preserves the parallel computing advantages of CNNs while addressing the drawbacks of conventional WNNs, such as feature discontinuity and strong manual dependency.

The main contributions of this work are as follows: a new CNN model is developed to achieve end-to-end fault diagnosis. It directly processes raw signal data, eliminating the cumbersome signal processing and feature selection steps typical in traditional fault diagnosis, thereby simplifying the diagnostic process and enhancing both efficiency and accuracy. Furthermore, a novel wavelet convolution kernel is designed, retaining the multi-scale feature extraction capability of discrete wavelet transforms (DWTs) while enabling wavelet feature optimization through backpropagation. Combined with the local feature extraction ability of CNN, this design enhances the model's capacity to capture multi-scale information, thereby improving its fault recognition and classification performance.

II. OPEN-CIRCUIT FAULT ANALYSIS OF NPC THREE-LEVEL INVERTERS

In NPC three-level inverters, when one or more power devices, such as insulated gate bipolar transistors (IGBTs), experience an open-circuit fault, the original operating state of these power devices will change. This alteration directly affects the inverter's output characteristics, resulting in abnormal fluctuations in parameters such as output voltage

and current. These anomalies further impact the performance of the connected motor, leading to increased torque ripple and a significant decline in overall system performance.

The topology of the NPC three-level inverter is shown in Fig. 1. The NPC three-level inverter consists of 12 power transistors, denoted as $S_{x1} \sim S_{x4}$ ($x = a, b, c$), where each phase contains four power switches. The operating states of P, O and N are realized by different combinations of power switches. As shown in Fig. 2(a), in state P, switch S_{a1} and S_{a2} are turned on, allowing current to flow from the positive terminal to the load or return through a diode to the positive terminal. In states O and N, the current paths pass through S_{a2} or S_{a3} , and S_{a3} and S_{a4} , respectively, as shown in Fig. 2(b) and Fig. 2(c). Each module must conduct at least once during each cycle to ensure the normal flow of current.

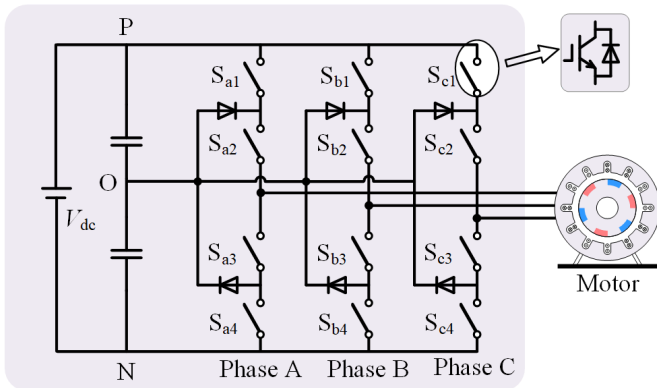


Fig. 1. Neutral Point Clamped Three-level Inverter.

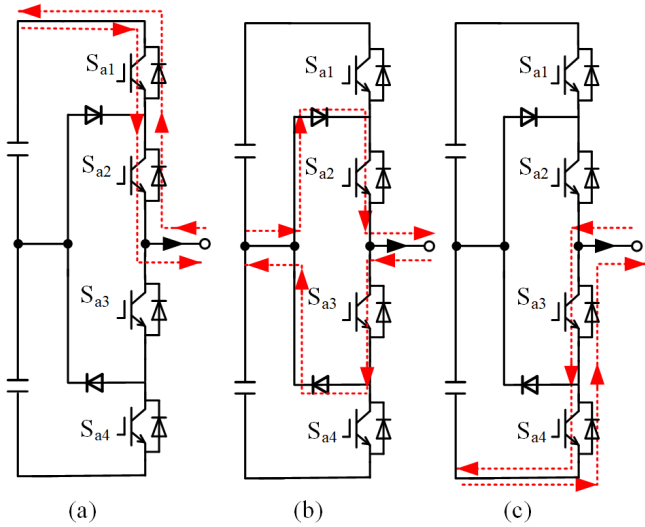


Fig. 2. Current loop of the normal operating state. (a) P state. (b) O state. (c) N state.

When an open-circuit fault occurs in any of the switches, the current waveform will become distorted. By monitoring the current waveform over one complete cycle, it is possible to determine the status of the internal switching devices and locate the fault. Under typical conditions, if an open-circuit fault occurs, it generally involves only one switch, and the number of simultaneously faulty switches does not exceed two. Fig. 3(a) shows the current waveform under normal conditions.

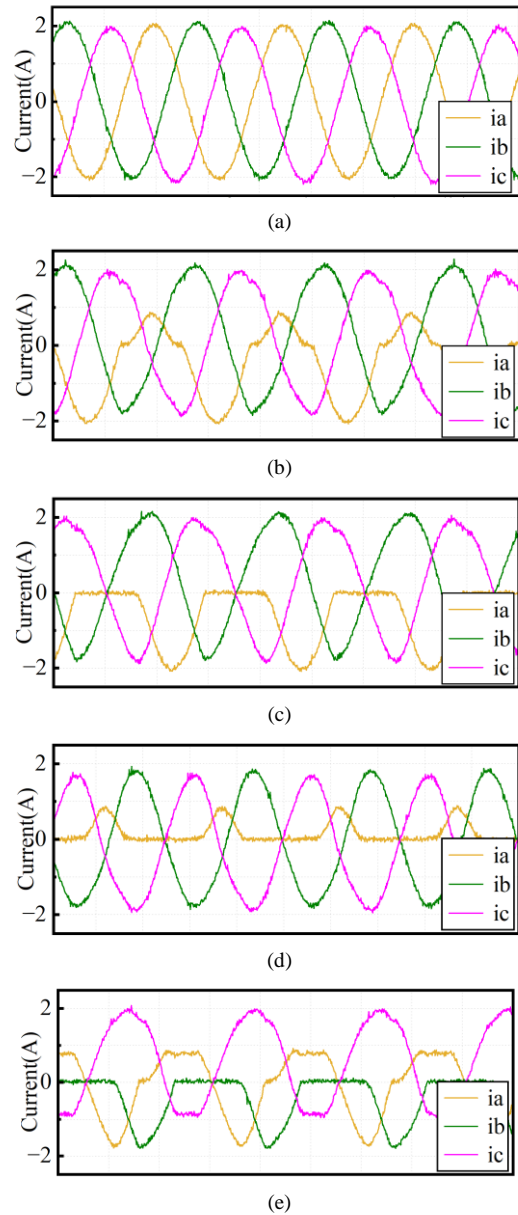


Fig. 3. Current waveform of inverter with open-circuit fault. (a) Current waveform under normal conditions. (b) Current waveform under S_{a1} fault. (c) Current waveform under S_{a2} fault. (d) Current waveform under $S_{a1}S_{a3}$ fault. (e) Current waveform under $S_{a1}S_{b2}$ fault.

Taking phase A as an example, when switch S_{a1} is in an open-circuit fault condition, it is equivalent to the inverter losing only the P state for phase A, while the O and N states remain unaffected. As a result, the inverter's output current can operate normally during the negative half-cycle. However, due to the presence of the freewheeling diode, only a small portion of the current exists during the positive half-cycle, as shown in Fig. 3(b). When switch S_{a4} experiences an open-circuit fault, the situation is the opposite of S_{a1} . The inverter loses the N state for phase A, while the O and P states remain unaffected. In this case, the inverter's output current operates normally during the positive half-cycle, while in the negative half-cycle, the presence of anti-parallel diodes allows freewheeling current to flow under fault conditions, resulting in current distortion. When switch S_{a2} encounters an open-

circuit fault, the inverter's phase A loses both the P and O states, while the N state remains intact. Consequently, the output current of the inverter is present only during the lower half-cycle, as illustrated in Fig. 3(c). Similarly, when switch S_{a3} experiences an open-circuit fault, the situation is the opposite of S_{a2} . The analysis for single switch open-circuit faults in the other phases is similar.

For double switch faults, this article takes S_{a1} and S_{a3} , as well as S_{a1} and S_{b2} , as examples to analyze their fault current characteristics. When switches S_{a1} and S_{a3} fail simultaneously, due to the symmetry of the NPC three-level inverter, the fault characteristics can be approximated as the linear superposition of the individual faults of switches S_{a1} and S_{a3} . When phase A is in the P state and the current direction is positive, the positive current flows from the capacitor midpoint through the upper clamping diode and S_{a2} to the AC side. Under fault conditions, the magnitude of the positive current is lower than its normal operating value. When phase A is in the P or N state and the current direction is negative, the current flows through two anti-parallel freewheeling diodes from the AC side to the DC side. However, due to the inability of the lower bridge switches to conduct negative current, the negative current in phase A is zero, as shown in Fig. 3(d). Based on the above analysis, when switch S_{a1} is faulty, it affects the P state of phase A, causing the positive current to flow through the upper clamping diode and S_{a2} to the AC side. This leads to a distortion in the positive current, although it is not completely zero. On the other hand, when S_{b2} fails, both the P and O states of phase B are fully compromised, resulting in an inability for the positive current to flow, and the positive current output of phase B becomes zero. At this time, both phase A and phase B exhibit abnormal current characteristics, manifesting as current distortion under the corresponding states. Due to the open-circuit faults in both phases A and B, the neutral point voltage becomes unbalanced, which also

causes fluctuations in the output current of phase C, as shown in Fig. 3(e).

III. FAULT DIAGNOSIS STRATEGY

A. Fault Diagnosis Model

In the diagnosis of open-circuit faults in NPC three-level inverters, the three-phase fault currents are typically used as the primary diagnostic basis, and these fault signals are represented as one-dimensional time series data. Traditional CNN networks are designed to handle two-dimensional inputs, and converting one-dimensional fault signals into matrix form can disrupt their original temporal structure, thereby weakening the expression of fault characteristics and reducing the accuracy of fault detection and classification. Therefore, this article adopts a 1D CNN network architecture for fault diagnosis. The amplitude characteristics of the one-dimensional fault current can effectively reflect different open-circuit fault modes, making it a valuable reference for fault diagnosis. However, when using 1D CNN for fault diagnosis, the diversity and reliability of the extracted features are critical to achieving high accuracy. Relying solely on current amplitude features is often insufficient for accurately diagnosing complex faults, as it lacks the capacity to fully represent the intricate dynamics associated with different fault scenarios.

To further enhance the accuracy and robustness of fault diagnosis, the article introduces an end-to-end wavelet kernel neural network. As illustrated in Fig. 4, the network mainly consists of wavelet convolutional layers, convolutional layers, pooling layers, and fully connected layers.

Wavelet transforms are widely used in digital signal processing. In practical applications, due to limitations in computational resources and storage, the DWT is often employed. The wavelet convolutional kernel is based on the

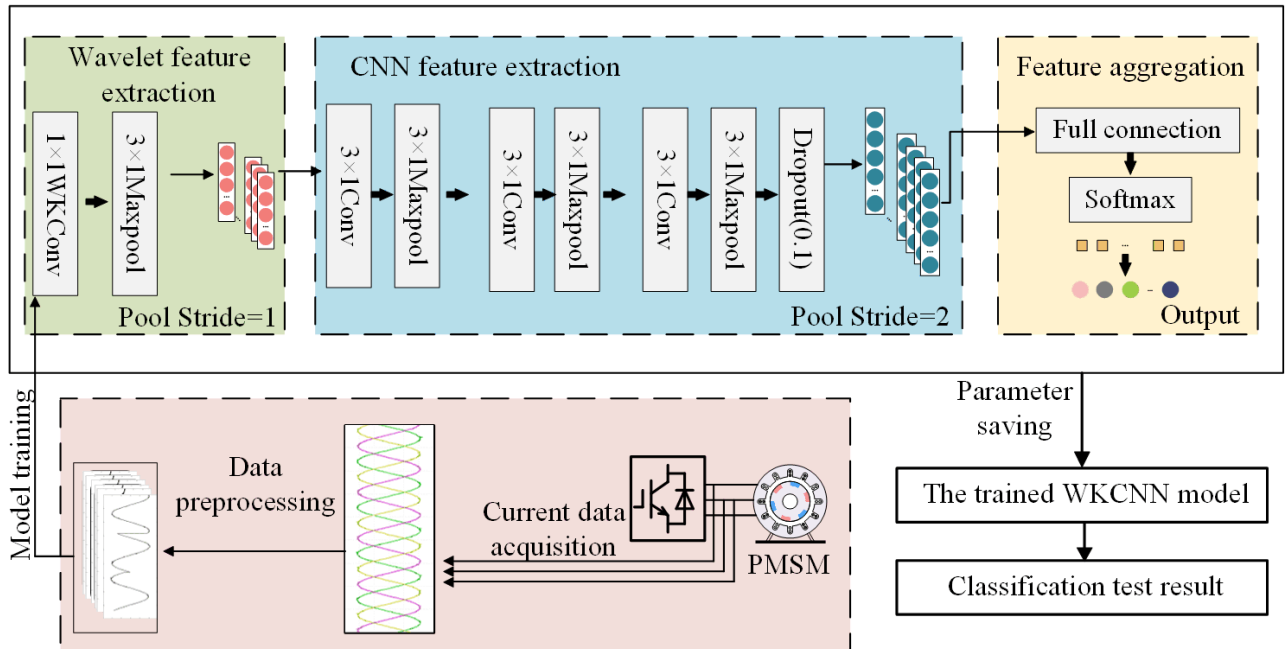


Fig. 4. Structure of WKCNN.

principles of DWT, which decomposes the data into a series of approximation coefficients and detail coefficients. The approximation coefficients represent the signal on a coarser time scale, while the detail coefficients capture high-frequency information or fluctuations at that scale. The mathematical expression for decomposing a one-dimensional signal using DWT is as follows:

$$\begin{cases} s_{1n} = \sum_j l_{j-2n} s_j \\ d_{1n} = \sum_j h_{j-2n} s_j \end{cases} \quad (1)$$

where the input signal $s = \{s_j\}$ ($j \in z$) represents decomposed by wavelet transform to obtain the approximation coefficients $s_1 = \{s_{1n}\}$ ($n \in z$) and detail coefficients $d_1 = \{d_{1n}\}$ ($n \in z$); z represents the signal length, and l and h represent the low-pass and high-pass filters of an orthogonal wavelet, respectively.

In this paper, a parameterized wavelet kernel is employed to replace one convolutional layer in a conventional CNN. The approach is based on the principles of the classical wavelet transform. The Haar wavelet basis is used for initialization in the CNN framework. The mother wavelet be denoted as $\psi(t)$; the parameterized wavelet kernel is defined as:

$$\psi_{a,b}(t) = \frac{1}{\sqrt{a}} \psi\left(\frac{t-b}{a}\right) \quad (2)$$

where a (> 0) denotes the scale factor that determines the extension or compression of the wavelet, and b denotes the translation factor that determines the wavelet's position in the time domain. To ensure that a remains positive, logarithmic parameterization is adopted. An unconstrained parameter α is introduced such that $a = \exp(\alpha)$.

In the design of the wavelet kernel, t is first sampled in the discrete time domain, and the sampling points are defined as:

$$t_k = -\frac{K-1}{2} + k, \quad k = 0, 1, \dots, K-1 \quad (3)$$

where K denotes the wavelet kernel length, and k denotes the index of the convolution kernel in the spatial domain.

At each sampling point t_k , the numerical computation of the discrete wavelet kernel, based on the scale factor a and the translation factor b , can be expressed as:

$$f_k = \psi_{a,b}(t_k) = \frac{1}{\sqrt{a}} \psi\left(\frac{t_k - b}{a}\right), \quad k = 0, 1, \dots, K-1 \quad (4)$$

All sampled values can be combined into a vector form:

$$\mathbf{f} = [f_0, f_1, \dots, f_{K-1}] \in \mathbb{R}^K \quad (5)$$

To avoid numerical amplitude instability, further normalization is applied to \mathbf{f} :

$$f'_k = \frac{f_k}{\sum_{j=0}^{K-1} |f_j|}, \quad k = 0, \dots, K-1 \quad (6)$$

Based on the discretization with a wavelet kernel of length K , the normalized vector f'_k is extended to form the convolutional layer weight tensor W [26], namely:

$$W_{i,j,k} = f'_k, \quad \forall i \in \{1, \dots, C_{out}\}, j \in \{1, \dots, C_{in}\}, k \in \{1, \dots, K\} \quad (7)$$

where i denotes the index of the output channel, j denotes the index of the input channel, C_{in} denotes the number of input channels, and C_{out} denotes the number of output channels.

For the input signal x , the convolution operation can be represented as:

$$y = x * W \quad (8)$$

where $*$ denotes the convolution operation. The weight W is composed of f'_k , and f'_k depends on the scale factor a and the translation factor b . During the backpropagation process, gradients are computed using the chain rule:

$$\begin{aligned} \frac{\partial L}{\partial \alpha} &= \sum_{i,j,k} \frac{\partial L}{\partial W_{i,j,k}} \cdot \frac{\partial W_{i,j,k}}{\partial a} \cdot \frac{\partial a}{\partial \alpha}, \\ \frac{\partial L}{\partial b} &= \sum_{i,j,k} \frac{\partial L}{\partial W_{i,j,k}} \cdot \frac{\partial W_{i,j,k}}{\partial b} \end{aligned} \quad (9)$$

where L denotes the loss function.

The above gradient computation permits parameters α and b to be dynamically adjusted via gradient descent, thereby achieving adaptive optimization of the wavelet kernel. This mechanism not only preserves the mathematical properties of the wavelet transform but also endows the model with the ability to automatically adjust the filter shape according to task requirements, thereby enhancing the flexibility of feature extraction.

The convolution layer is used to extract local features from the input data. The convolution kernel performs a weighted summation on local regions of the input data, generating new feature maps. Different convolution kernels represent different features, thus utilizing multiple convolution kernels enhances the feature extraction capability of the model, enabling the network to learn richer features. The convolution operation is mathematically expressed as follows:

$$x'_j = f\left(\sum_{i \in M_j} x_i^{l-1} w'_{ij} + b'_j\right) \quad (10)$$

where M_j denotes the dimension of the input data, l represents the layer number of the network, x_i^{l-1} is the input data involved in the convolution, w'_{ij} is the weight matrix, and b'_j indicates the bias matrix. The function $f(\cdot)$ is the activation function, and in this work, the ReLU activation function is used.

The pooling layer is primarily used to reduce the spatial dimensions of the feature maps, thereby decreasing computational complexity while retaining important feature information. This enhances the training efficiency and generalization ability of the model. In this article, max pooling is employed. Max pooling selects the maximum value from the local receptive field to preserve the most significant features, which reduces the computational burden of the model and effectively prevents overfitting. The pooling operation is mathematically expressed as follows:

$$p_{l+1}(y_i) = \max_{(n-1)H+1 \leq i \leq nH} \{q_{l,m}(i)\} \quad (11)$$

where $q_{l,m}(i)$ represents the value of the i -th neuron in the m -th filter of the l -th layer, H is the width of the pooling region, and $p_{l+1}(y_i)$ denotes the output value after pooling.

The fully connected layer is connected to every neuron in the preceding layer, combining the fault features extracted by

the convolutional and pooling layers. It then converts these features into a probability distribution for each category using the Softmax function. The fully connected layer is mathematically expressed as follows:

$$y^k = f(w^k x^{k-1} + b^k) \quad (12)$$

where k is the layer number of the network, y^k is the output value of the fully connected layer, w^k represents the weight coefficients, x^{k-1} is the fault feature vector, and b^k denotes the bias term. The function $f(\cdot)$ is the Softmax activation function, which is commonly used for multi-class classification tasks. Its role is to convert the network's output values into a probability distribution, where each class probability lies between 0 and 1, and the sum of the probabilities for all classes is equal to 1, thereby providing an intuitive representation of the predicted probability for each category. The Softmax function is mathematically expressed as follows:

$$\sigma(y_i) = \frac{e^{y_i}}{\sum_{j=1}^M e^{y_j}} \quad (13)$$

where y_i represents the input value of the i -th neuron in the output layer of the neural network, M is the total number of classes in the classification task, e^{y_i} denotes the exponential value of the input y_i , and $\sum_{j=1}^M e^{y_j}$ represents the sum of the exponentials of all output values y , which is used to normalize each output into a probability.

Unlike traditional multi-step processing methods, WKCNN adopts an end-to-end architecture that directly extracts multi-scale, multi-resolution time-frequency features from the raw fault current signals, without the need for extensive manual feature engineering. By integrating the multi-resolution analysis capability of wavelet transforms, the wavelet neural network can not only capture local features of the signal but also effectively extract fault characteristics across different frequency components, ensuring that important information is preserved.

B. Fault Diagnosis Process

The fault diagnosis process based on WKCNN is illustrated in Fig. 5, with the specific steps detailed as follows:

Step 1: fault signal acquisition involves collecting the three-phase current data (i_a , i_b , i_c) from the NPC three-level inverter while driving a PMSM. These current signals are used as the input for the fault diagnosis process. The collected signals contain specific features corresponding to various fault modes, providing essential data for diagnosing faults.

Step 2: slicing the three-phase current signals into multiple time segments, forming the input dataset. The three-phase currents, as the raw fault features for network input, are processed to ensure that the temporal information and the correlations between the phase currents are preserved.

Step 3: the WKCNN model receives the training dataset with fault characteristics. WKCNN, with its unique wavelet kernel convolutional structure, combines multi-resolution feature extraction with convolution operations to progressively

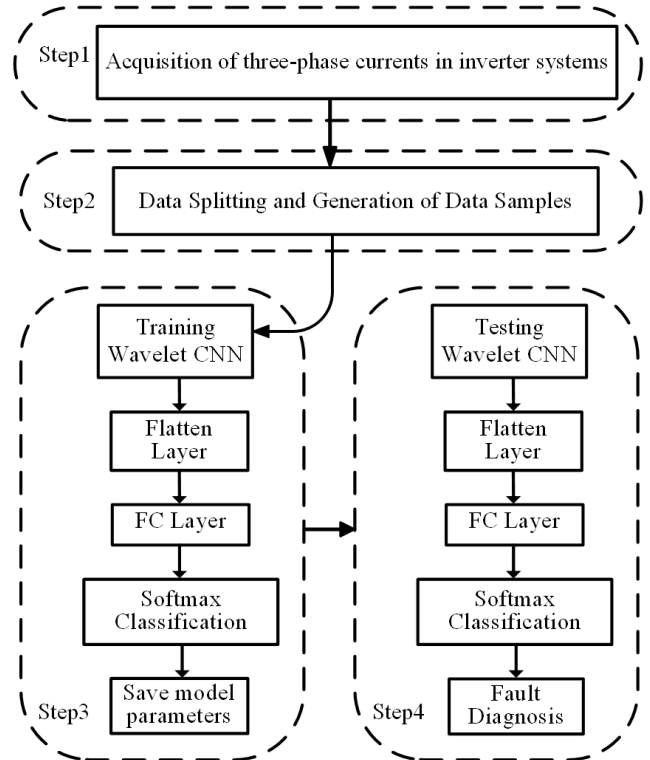


Fig. 5. Fault diagnosis based on WKCNN.

learn fault features from the signals. During training, the network extracts the time-frequency features of the fault signals through a hierarchical learning structure, while continuously adjusting network parameters and optimizing weight allocation using the backpropagation algorithm. The final layer employs a Softmax classifier to map the extracted features to specific fault categories, thereby enabling accurate classification of different fault types.

Step 4: The fault sample test set is used to evaluate the model. The fault data samples are fed into the trained WKCNN model, which processes and classifies these test samples. The model's fault diagnosis accuracy is evaluated under various conditions for different fault types, allowing analysis of its generalization capability and robustness. This process verifies the practical effectiveness of the model.

IV. EXPERIMENTAL VALIDATIONS

A. Experimental Platform

To verify the applicability of the proposed method under different operating conditions, an experimental platform was set up as shown in Fig. 6. The experimental setup consists of two PMSMs directly connected via a coupling. One PMSM acts as the test motor, while the other serves as the load motor. The parameters of the PMSMs used in the experiments are detailed in Table I. The experimental controller used is the RTU-BOX206 real-time digital controller. The control system model is built in MATLAB/Simulink and compiled into executable code for the RTU-BOX206, enabling online parameter adjustment. To simulate fault conditions, the control signal of the power switch in the inverter is cut off to collect fault signals, followed by fault diagnosis experiments

to verify the effectiveness of the proposed fault diagnosis method in practical applications.

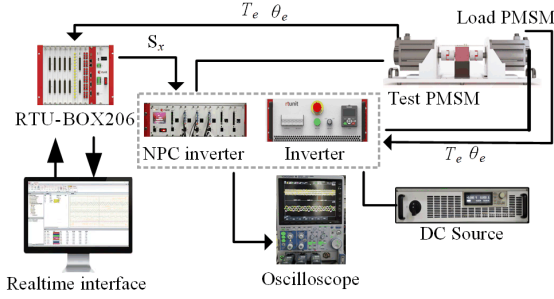


Fig. 6. Experiment platform.

TABLE I
PARAMETERS OF PMSM

| Parameters | Values |
|---|------------------------|
| Rated power/kW | 5.5 |
| Rated line voltage/V | 380 |
| Rated line current/A | 12 |
| Rated speed/RPM | 1500 |
| Rated torque/(N m) | 35 |
| Counter-electromotive force/(V/(1000 r min ⁻¹)) | 181 |
| Rotor inertia/(kg·m ²) | 12.25×10 ⁻³ |
| Winding inductance/mH | 4 |
| Winding resistance/Ω | 0.62 |
| Number of pole pairs | 4 |

The experimental computing platform used an NVIDIA GeForce GTX 1080 with Max-Q Design GPU, with a memory capacity of 16 GB. The programming language used was Python, and the deep learning framework chosen was Pytorch, version 1.13.1. Algorithm development and execution were both performed in the PyCharm integrated development environment. During model training, the Adam optimizer was employed with a learning rate of 0.0001 and a batch size of 128. The dataset was split into a training set and a testing set in a ratio of 8:2. Each training session involved 50 epochs, using cross-entropy as the loss function. The experiments were repeated multiple times to ensure stability and reliability of the results.

B. Experimental Results and Analysis

Fault current data was collected under RL Load ($R=10\ \Omega$, $L=10\ \text{mH}$) as well as during the operation of a PMSM at different speeds (400, 500, 600 r/min) and different loads (1.75 N m and 3.5 N m, referred to as PMSM Load 1 and PMSM Load 2, respectively). The detailed conditions are shown in Table II. For each fault mode, the three-phase current signals were collected with a sampling length of 125k. Subsequently, these current signals were sliced, resulting in feature vectors of length 3000 for each phase. Each fault data collection produced 41 samples under the same fault mode, with each sample containing 9000 data points. To increase the sample size, data collection was repeated three times for each operating condition, ultimately yielding 123 samples per fault mode. For single switch fault modes, a total of 1599 samples were obtained for model training and testing.

TABLE II
OPERATING CONDITION TYPE TABLE

| Dataset | Operating Condition | | |
|---------|---|----------------|----------------|
| A | PMSM Load1 | | |
| B | PMSM 400 r/min | PMSM 500 r/min | PMSM 600 r/min |
| C | PMSM Load1 | PMSM Load2 | RL Load |
| D | Single switch failure & Double switch failure | | |

The depth of the network has a significant influence on its feature extraction ability. The proposed WKCNN model allows adjustment of the network depth by changing the number of convolutional layers. This article conducted validation and analysis of the WKCNN model's performance under different network depths. The number of convolutional layers was set from CNN 2 to 5, and the models were named WKCNN-2, WKCNN-3, WKCNN-4, and WKCNN-5, respectively, to evaluate the performance at varying depths. The experiments were conducted under the conditions of Dataset A, with the model utilizing the Harr wavelet.

Fig. 7 and Fig. 8 illustrate the performance of WKCNN models with different depths on the test set. According to the accuracy variation curves shown in Fig. 7, it is evident that network depth has a significant impact on model performance. The shallow network, WKCNN-2, exhibits a slower growth in accuracy during the early stages of training, and its final accuracy is noticeably lower compared to deeper networks, indicating weaker feature extraction capability.

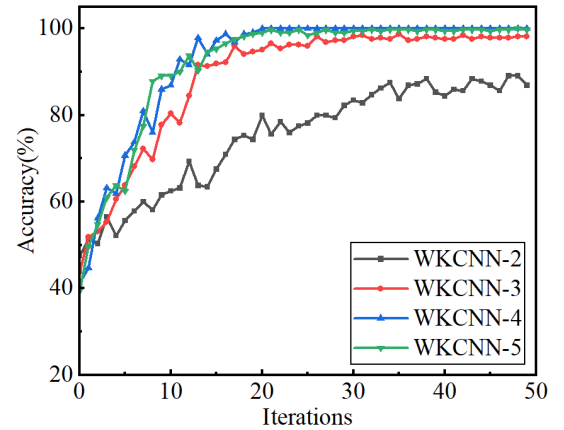


Fig. 7. Performance of WKCNN models with different network depths.

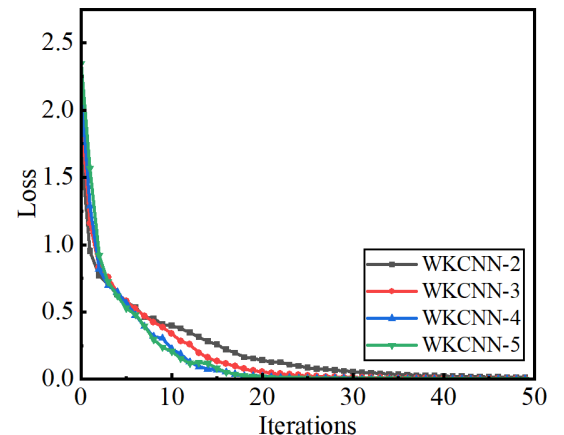


Fig. 8. Loss curves WKCNN models with different network depths.

WKCNN-3 and WKCNN-4 show faster convergence rates and higher accuracy, as the increased depth enhances the ability to extract features, leading to significantly better performance on the test set compared to the shallow network. The final performance of WKCNN-5 is similar to that of WKCNN-4, indicating that further increasing the depth provides limited improvements in accuracy. Increasing network depth can effectively enhance the model's feature extraction ability and accuracy, but once the depth reaches a certain point, additional depth yields diminishing returns in performance gains. Furthermore, overly deep networks may result in a significant increase in computational costs and are more prone to overfitting, which can reduce generalization capability in practical applications.

Based on the experimental results, WKCNN-4 achieves a good balance between accuracy and computational efficiency, effectively extracting fault features without wasting computational resources due to excessive depth. Therefore, WKCNN-4 is selected as the diagnostic network model in this article.

The optimal network architecture determined from the above experiments is illustrated in Fig. 4. This network consists of four convolutional layers, each followed by a corresponding max-pooling layer. The first wavelet kernel convolutional layer has an input channel of 1 and an output channel of 32, with a kernel size of 1 and a stride of 1. Down sampling is performed using a max-pooling layer with a pool size of 3 and a stride of 1. The subsequent convolutional layers are configured with output channels of 64, 128, and 256, respectively, with a kernel size of 3 and a stride of 1. Each convolutional layer is followed by a max-pooling layer with a pool size of 3 and a stride of 2. To prevent overfitting during the training process, a Dropout layer with a dropout rate of 0.1 is added at the end of the network.

To verify the applicability of the proposed model for fault diagnosis under various operating conditions, experiments were conducted involving different speeds and loads of the PMSM, as well as double switch faults that may occur in the NPC three-level inverter. Due to the large number of possible double switch fault types, four representative fault types were selected for analysis: $S_{a1}S_{a2}$, $S_{a1}S_{a3}$, $S_{a1}S_{b1}$, and $S_{a1}S_{b2}$. A dataset was constructed by combining these double switch faults with single switch faults. The different operating conditions correspond to datasets B, C, and D, respectively, to further evaluate the model's diagnostic capability across various fault scenarios.

The fault diagnosis accuracy of the model under different speed conditions, as shown in Fig. 9, is very similar, with a final accuracy reaching 100%. The model converges rapidly within the first 15 epochs and remains stable thereafter. This indicates that the model can quickly learn and adapt to the feature extraction requirements under different speed conditions. Whether at 400 rpm or higher speeds of 500 rpm or 600 rpm, the model demonstrates consistent feature extraction capabilities. The model exhibits good robustness, handling fault signals under different speed conditions with little impact from speed variations. This confirms that the

model maintains stable fault diagnosis performance across different speed operating conditions.

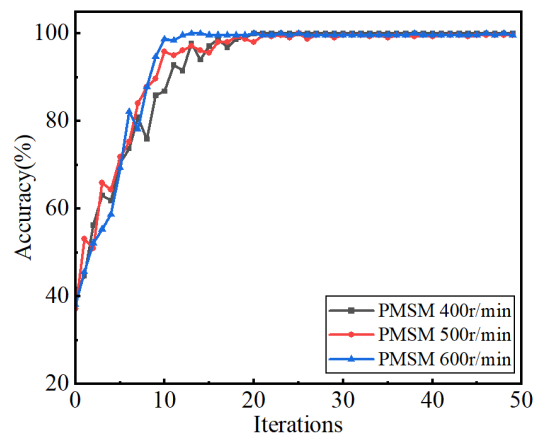


Fig. 9. Performance of WKCNN Model under different RPMs.

As shown in Fig. 10, the fault diagnosis performance under different load conditions is consistent, with a final accuracy of 100% in all cases. Under RL load conditions, the model shows a very fast convergence rate, reaching nearly 100% accuracy within the first 5 epochs. Under motor load conditions, the convergence rate is slightly slower but still reaches stable high accuracy around 15 epochs. This indicates that the model demonstrates good robustness across different load conditions, effectively adapting to variations in load scenarios, accurately extracting fault features, and performing classification. These results prove the model's adaptability and stability under a variety of load conditions.

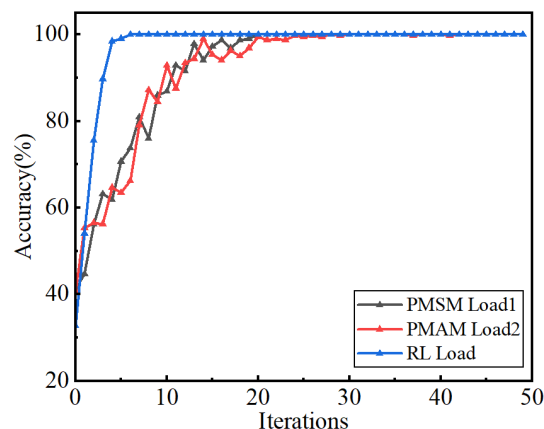


Fig. 10. Performance of WKCNN Model under different loads.

The training and testing performance of the model under single and double switch fault conditions is similar, as shown in Fig. 11, with training and testing accuracy increasing almost synchronously and eventually reaching a high accuracy of 100%. The accuracy curves for both training and testing rise rapidly and converge within the first 10 epochs, indicating that the model exhibits good learning and generalization capabilities when handling double switch fault data.

To further verify the performance of the proposed method, random forest (RF), long short-term memory network (LSTM), and 1D CNN were selected as comparison

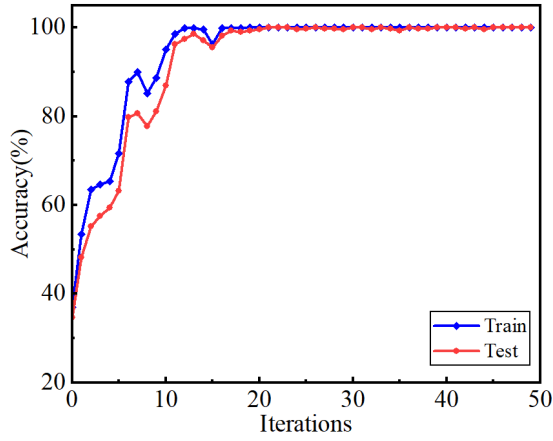


Fig. 11. Performance of WKCNN Model under single and double switch fault conditions.

algorithms. As shown in Fig. 12, the numbers on the horizontal axis represent different test conditions, including the PMSM under various speeds, different loads, RL load conditions, as well as combinations of single and double switch faults. As illustrated in Fig. 12, the proposed WKCNN model outperforms the other comparison algorithms in fault diagnosis across all tested conditions and exhibits good classification ability in each dataset experiment. Overall, WKCNN demonstrates high robustness and accuracy across all experimental scenarios, showing its superiority in fault diagnosis tasks.

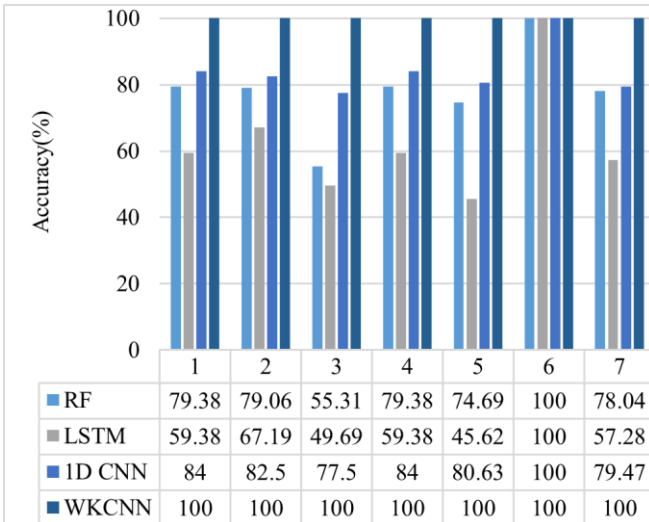


Fig. 12. Performance of WKCNN, RF, LSTM, and 1D CNN under different operating conditions.

Parameters, floating-point operations (FLOPs), and memory required during node inference are key metrics for evaluating model complexity. Table III presents a comparison of various network models on Dataset A. In the table, the RF model is configured with 500 trees and a tree depth of 20. The LSTM structure is set as 256-256-256-13. An attention mechanism maps the LSTM output at each time step to a scalar score via a fully connected layer with associated weights and bias. The 1D CNN model employs the same number of layers and parameter configuration as WKCNN.

TABLE III
COMPLEXITY COMPARISON OF DIFFERENT MODELS

| Model | Parameters | FLOPs | Memory (GB) |
|-------|------------|-----------|-------------|
| RF | 134722 | 16057 | 0.0219 |
| LSTM | 10536462 | 10542592 | 0.0402 |
| 1DCNN | 7600909 | 394192384 | 0.0300 |
| WKCNN | 3863567 | 390455040 | 0.0147 |

It is observed that the parameter count of WKCNN is much lower than that of the LSTM, and its memory usage is only 0.0147 GB, which significantly reduces the hardware resources required for deployment. Moreover, WKCNN achieves excellent diagnostic accuracy while maintaining low model complexity. Overall, the performance of WKCNN is superior to that of RF and 1D CNN. In particular, compared with the 1D CNN, WKCNN greatly reduces the parameter count and nearly halves the memory usage. This indicates that, while retaining convolutional feature extraction capability, the multi-scale representation via wavelet convolution effectively enhances resource utilization efficiency.

C. Model Result Visualization

Visualization of model results refers to representing the output of machine learning or deep learning models in graphical form, allowing for a more intuitive understanding and evaluation of model performance. Common visualization methods include confusion matrices, visualization of neural network structures, and presentation of prediction results. To further analyze the diagnostic results and evaluate the model's performance in fault classification and fault data processing, this article introduces the uniform manifold approximation and projection (UMAP) dimensionality reduction algorithm to visualize the feature distribution of test samples within the model. Taking Dataset A as an example, Fig. 13 shows the visualization results, where the horizontal axis represents Dimension 1, and the vertical axis represents Dimension 2.

From Fig. 13(a), it can be observed that different fault categories of input data are not well distinguished in the two-dimensional space. It can be seen from Fig. 13(b) that the UMAP dimensionality reduction results show good separability among different fault signals. Data points from different categories form distinct clusters in the two-dimensional space, with most clusters well separated from each other. This indicates that the model has strong classification capabilities. However, some categories are positioned relatively close to each other, suggesting a certain degree of classification ambiguity, indicating room for further optimization in distinguishing these categories. Overall, the model demonstrates high accuracy and robustness in identifying fault signals across different categories.

D. Analysis of Feature Extraction Process

In order to more intuitively reveal the regions where the model focuses on fault features, normal, and S_{a1} fault cases are selected as examples. The Grad-CAM method [27] is employed to compute attribution values on the model's fourth

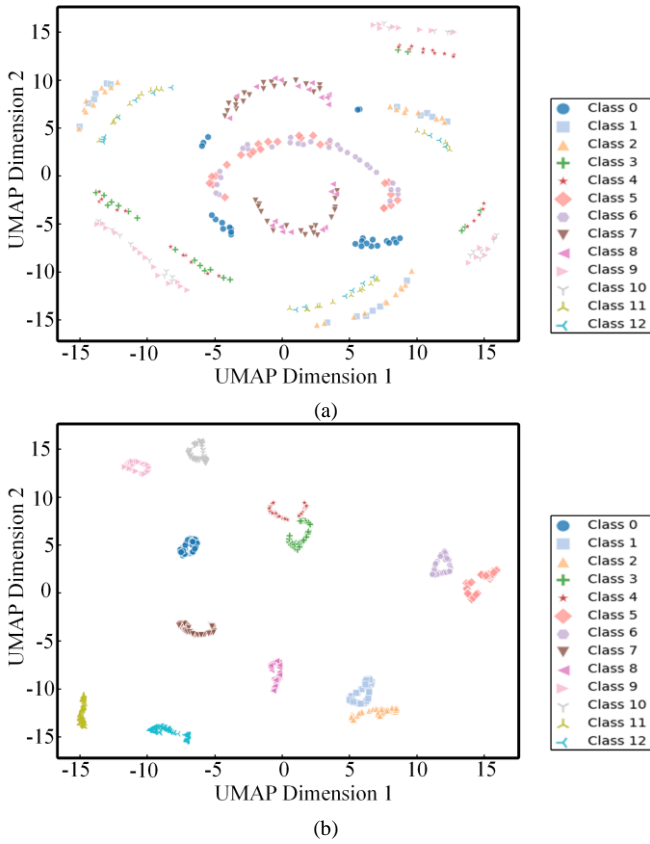


Fig. 13. Visualization of model training process. (a) UMAP visualization of input. (b) UMAP visualization of output.

layer (Wconv4) for interpretability analysis. In the visualization, the output data of Wconv4 is displayed as line subplots, while the Grad-CAM attribution values are presented as heatmap subplots, as shown in Figs. 14 and 15. Bright bands in the heatmaps indicate that the model is more sensitive to the corresponding label during those time intervals, contributing positively to classification. Dark regions indicate a weaker contribution. The tick marks on the *x*-axis denote the boundaries of the three-phase currents in the Wconv4 output.

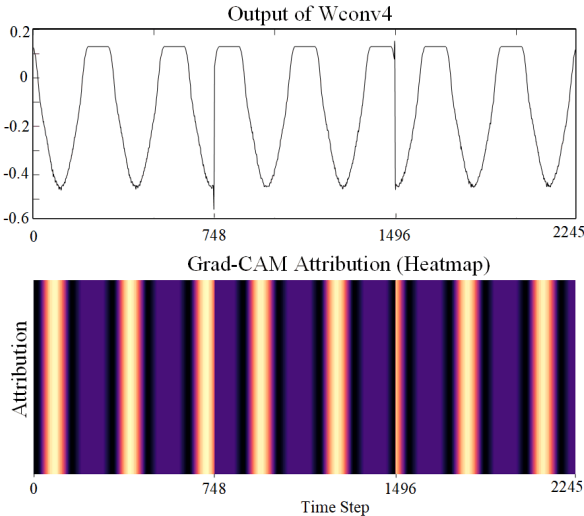


Fig. 14. Feature extraction and Grad-CAM analysis in Normal.

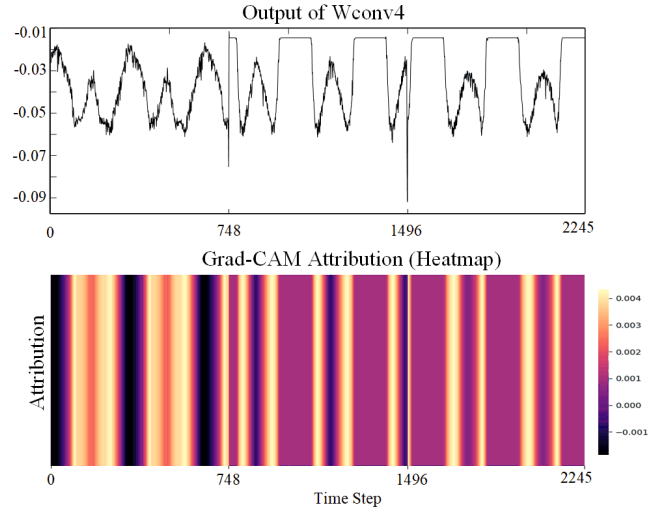


Fig. 15. Feature extraction and Grad-CAM analysis in S_{a1} .

From the figures, it is observed that under normal inverter operation the overall waveform is stable and exhibits periodicity. The attribution values range from approximately -0.002 to 0.008 , with positive values dominating. The attribution heatmap displays periodic bright regions that correspond to the periodicity of the waveform. Under the S_{a1} fault condition, abnormal fluctuations are observed in the signal from time steps 0 to 748. This region corresponds to the phase A current. The attribution values in this region range from approximately -0.001 to 0.004 , which is lower than the maximum attribution values observed under normal conditions. Compared to other regions, this area is highlighted, indicating that higher attention is paid to it during S_{a1} fault classification. In the subsequent time interval, the attribution values remain positive and exhibit periodic bright regions, indicating that the periodic features of the recovered waveform are also captured. This demonstrates the model’s comprehensive ability to capture fault characteristics.

These visualization results indicate that although the WKCNN model is an end-to-end trained black box, feature extraction and Grad-CAM analysis show that the model extracts different features for the corresponding fault types in fault samples. At the same time, Grad-CAM attribution also displays different highlighted regions. This indicates that the features in that segment play a decisive role in classifying open-circuit faults in inverter. These findings are consistent with the typical physical characteristics of open-circuit faults in inverters.

V. CONCLUSION

This article proposes an intelligent method for diagnosing open-circuit faults in NPC three-level inverters. By applying wavelet convolutional kernels, the model is capable of deeply extracting fault features, allowing efficient applicability across multiple operating conditions. The WKCNN model possesses an end-to-end structure, enabling direct processing of raw current signals without relying on manually designed features, which effectively enhances the automation level of

the diagnostic process. In tests under various operating conditions, the model demonstrated good diagnostic capabilities, exhibiting good stability and broad applicability. Experimental results show that this method can effectively handle fault data, outperforming traditional machine learning and some deep learning models in diagnostic efficiency, which shows the superiority of the proposed model.

REFERENCES

- [1] T. B. Yu, W. C. Wan, and S. X. Duan, "A Modulation Method to Eliminate Leakage Current and Balance Neutral-point Voltage for Three-level Inverters in Photovoltaic Systems," *IEEE Trans. on Industrial Electronics*, vol. 70, no. 2, pp. 1635–1645, Feb. 2023.
- [2] R. Sarker, A. Bhattacharya, and S. Debnath *et al*, "A Novel FPGA-driven HD-SPWM Architecture with Zero-sequence Voltage Insertion Strategy for Three-level NPC Inverter," *IEEE Trans. on Industrial Informatics*, vol. 20, no. 9, pp. 10814–10824, Sept. 2024.
- [3] A. S. Gardouh, S. Abulanwar, and F. J. Deng *et al*, "Novel Fuzzy-based Open-switch Fault Detection Scheme of Voltage Source Inverter Induction Motor Drive," *IEEE Trans. on Power Electronics*, vol. 39, no. 11, pp. 14961–14973, Nov. 2024.
- [4] W. T. Huang, J. C. Du, and W. Hua *et al*, "A Hybrid Model-based Diagnosis Approach for Open-switch Faults in PMSM Drives," *IEEE Trans. on Power Electronics*, vol. 37, no. 4, pp. 3728–3732, Apr. 2022.
- [5] J. Fang, M. Y. Li, and S. C. Ding *et al*, "Circulating Current-based Open-circuit Fault Diagnosis for Parallel Inverters," *IEEE Journal of Emerging and Selected Topics in Power Electronics*, vol. 12, no. 3, pp. 2902–2911, Jun. 2024.
- [6] Z. L. Zhang, G. Z. Luo, and Z. B. Zhang *et al*, "A Hybrid Diagnosis Method for Inverter Open-circuit Faults in PMSM Drives," *CES Transactions on Electrical Machines and Systems*, vol. 4, no. 3, pp. 180–189, Sept. 2020.
- [7] C. Yang, W. H. Gui, and Z. W. Chen *et al*, "Voltage Difference Residual-based Open-circuit Fault Diagnosis Approach for Three-level Converters in Electric Traction Systems," *IEEE Trans. on Power Electronics*, vol. 35, no. 3, pp. 3012–3028, Mar. 2020.
- [8] Q. T. An, L. Z. Sun, and K. Zhao *et al*, "Switching Function Model-based Fast-diagnostic Method of Open-switch Faults in Inverters without Sensors," *IEEE Trans. on Power Electronics*, vol. 26, no. 1, pp. 119–126, Jan. 2011.
- [9] U. M. Choi, H. G. Jeong, and K. B. Lee *et al*, "Method for Detecting an Open-switch Fault in a Grid-connected NPC Inverter System," *IEEE Trans. on Power Electronics*, vol. 27, no. 6, pp. 2726–2739, Jun. 2012.
- [10] W. T. Huang, J. C. Du, and W. Hua *et al*, "An Open-circuit Fault Diagnosis Method for PMSM Drives Using Symmetrical and DC Components," *Chinese Journal of Electrical Engineering*, vol. 7, no. 3, pp. 124–135, Sept. 2021.
- [11] X. Wu, C. Y. Chen, and T. F. Chen *et al*, "A Fast and Robust Diagnostic Method for Multiple Open-circuit Faults of Voltage-source Inverters Through Line Voltage Magnitudes Analysis," *IEEE Trans. on Power Electronics*, vol. 35, no. 5, pp. 5205–5220, May 2020.
- [12] U. M. Choi, J. S. Lee, and F. Blaabjerg *et al*, "Open-circuit Fault Diagnosis and Fault-tolerant Control for a Grid-connected NPC Inverter," *IEEE Trans. on Power Electronics*, vol. 31, no. 10, pp. 7234–7247, Oct. 2016.
- [13] R. Peugot, S. Courtine, and J. P. Rogon, "Fault Detection and Isolation on a PWM Inverter by Knowledge-based Model," *IEEE Trans. on Industry Applications*, vol. 34, no. 6, pp. 1318–1326, Nov.-Dec. 1998.
- [14] Y. Yan, J. Q. Wu, and Y. F. Cao *et al*, "An Open-circuit Fault Diagnosis Method for Three-level Neutral Point Clamped Inverters based on Multi-scale Shuffled Convolutional Neural Network," *Sensors*, vol. 24, no. 6, pp. 1745–1745, Mar. 2024.
- [15] B. Li, J. B. Cui, and Y. G. He *et al*, "Fault Diagnosis of Active Neutral Point Clamped Three-level Inverter based on Energy Spectrum Entropy and Wavelet Neural Network," *Transactions of China Electrotechnical Society*, vol. 35, no. 10, pp. 2216–2225, May 2020.
- [16] Q. Sun, X. H. Yu, and H. S. Li *et al*, "Adaptive Feature Extraction and Fault Diagnosis for Three-phase Inverter based on Hybrid-CNN Models Under Variable Operating Conditions," *Complex & Intelligent Systems*, vol. 8, no. 1, pp. 29–42, Feb. 2022.
- [17] T. Z. Wang, J. Qi, and H. Xu *et al*, "Fault Diagnosis Method based on FFT-RPCA-SVM for Cascaded-multilevel Inverter," *ISA transactions*, vol. 60, pp. 156–163, Jan. 2016.
- [18] S. H. Kim, D. Y. Yoo, and S. W. An *et al*, "Fault Detection Method Using a Convolution Neural Network for Hybrid Active Neutral-point Clamped Inverters," *IEEE Access*, vol. 8, pp. 140632–140642, Jul. 2020.
- [19] X. Deng, C. G. Wan, and L. Jiang *et al*, "Open-switch Fault Diagnosis of Three-phase PWM Converter Systems for Magnet Power Supply on EAST," *IEEE Trans. on Power Electronics*, vol. 38, no. 1, pp. 1064–1078, Jan. 2023.
- [20] W. B. Yuan, Z. G. Li, and Y. G. He *et al*, "Open-circuit Fault Diagnosis of NPC Inverter based on Improved 1-D CNN Network," *IEEE Trans. on Instrumentation and Measurement*, vol. 71, pp. 1–11, Apr. 2022.
- [21] J. Hang, X. M. Shu, and S. C. Ding *et al*, "Robust Open-circuit Fault Diagnosis for PMSM Drives Using Wavelet Convolutional Neural Network with Small Samples of Normalized Current Vector Trajectory Graph," *IEEE Trans. on Industrial Electronics*, vol. 70, no. 8, pp. 7653–7663, Aug. 2023.
- [22] Y. Zhao, C. She, and D. D. Li *et al*, "Inter-turn Short Circuit Diagnosis of Wound-field Doubly Salient Machine based on Multi-signal Fusion on Feature Level Under Extreme Conditions," *Transactions of China Electrotechnical Society*, vol. 38, no. 10, pp. 2661–2674, May 2023.
- [23] X. Y. Ren, Y. Qin, and B. Wang *et al*, "An Intelligent Multi-sensor Information Fusion Fault Diagnosis Method of Three-phase Motors based on Game Mapping Learning," *Transactions of China Electrotechnical Society*, vol. 38, no. 17, pp. 4633–4645, Sept. 2023.
- [24] X. M. Zhang, and C. B. Wen, "Fault Diagnosis of Rolling Bearings based on Dual-channel Transformer and Swin Transformer V2," in *Proc. of 2024 43rd Chinese Control Conference*, Kunming, China, Jul. 2024, pp. 4828–4834.
- [25] S. Q. Zhang, R. J. Wang, and Y. P. Si *et al*, "An Improved Convolutional Neural Network for Three-phase Inverter Fault Diagnosis," *IEEE Trans. on Instrumentation and Measurement*, vol. 71, pp. 1–15, 2022.
- [26] S. Mallat, "Group Invariant Scattering," *Communications on Pure and Applied Mathematics*, vol. 65, no. 10, pp. 1331–1398, Oct. 2012.
- [27] R. R. Selvaraju, M. Cogswell, and A. Das *et al*, "Grad-CAM: Visual Explanations from Deep Networks via Gradient-based Localization," in *Proc. of 2017 IEEE International Conference on Computer Vision*, Venice, Italy, pp. 618–626, Oct. 2017.



Guozheng Zhang (M'20) was born in Datong, China, in 1985. He received the B.S. degree from Tianjin University, Tianjin, China, in 2008, the M. S. degree from Tianjin University of Science and Technology, Tianjin, China, in 2011, and the Ph.D. degree from Tianjin University, Tianjin, China, in 2017, all in electrical

engineering.

He is currently an Associate Professor with the School of Electrical Engineering, Tiangong University, Tianjin, China, and also with the National Local Joint Engineering Research Center of Electrical System Design and Manufacturing. His research interests include electrical machines, multilevel converters and their control systems.



Menghui Li was born in Shandong, China, in 1998. He received the B.S. degree from Qufu Normal University, Rizhao, China, in 2021, in electrical engineering. He is currently working toward the Master degree in electrical engineering with the School of Electrical Engineering, Tiangong University,

Tianjin, China.

His research interests include fault diagnosis of multilevel converters and machine learning.



Xin Gu (M'19) was born in Tianjin, China, in 1980. He received the B.S., M.S. and Ph.D. degrees from Tianjin University, Tianjin, China, in 2003, 2006 and 2010, all in electrical engineering.

He is currently a professor with the School of Electrical Engineering, and with the National Local Joint Engineering Research Center of Electrical System Design and Manufacturing. He is also the Deputy Director with Electrical Machine System Research Institute of Tiangong University. His research interests include permanent magnet synchronous machines, power electronic converters and their control systems.



Wei Chen (M'12) was born in Shanxi, China, in 1977. He received the B.S., M.S., and Ph.D. degrees in electrical engineering from Tianjin University, Tianjin, China, in 2000, 2003, and 2006, respectively.

He is currently a Professor with the School of Electrical Engineering, Tiangong University, and the Vice President of the National Local Joint Engineering Research Center of Electric Machine System Design and Manufacturing, China. His research interests include electrical machines and drives, power electronics.